Cellular/Molecular

Excitability of Type II Cochlear Afferents

Catherine J. C. Weisz,[2] Elisabeth Glowatzki,[1,2] and Paul Albert Fuchs[1,2]

[1]Department of Otolaryngology–Head and Neck Surgery and [2]Solomon Snyder Department of Neuroscience, Johns Hopkins School of Medicine, Baltimore, Maryland 21205

Two types of sensory hair cells in the mammalian cochlea signal through anatomically distinct populations of spiral ganglion afferent neurons. The solitary inner hair cell ribbon synapse uses multivesicular release to trigger action potentials that encode acoustic timing, intensity, and frequency in each type I afferent. In contrast, cochlear outer hair cells (OHCs) have a far weaker effect on their postsynaptic targets, the type II spiral ganglion afferents. OHCs typically release single vesicles with low probability so that extensive summation is required to reach the relatively high action potential initiation threshold. These stark differences in synaptic transfer call into question whether type II neurons contribute to the cognitive perception of sound. Given the sparse and weak synaptic inputs from OHCs, the electrical properties of type II afferents are crucial in determining whether synaptic responses can sum to evoke an action potential to convey information to the cochlear nucleus. In the present work, dual-electrode recordings determined that type II afferents of rats have length constants that exceed the length of the distal, spiral process, enabling spatial summation from widespread OHCs. Focal application of tetrodotoxin localized the spike initiation zone to the type II proximal, radial process, near the spiral ganglion, in agreement with the high voltage threshold measured in the spiral process. These measured membrane properties were incorporated into a compartmental model of the type II neuron to demonstrate that neurotransmitter release from at least six OHCs is required to trigger an action potential in a type II neuron.

Key words: **auditory; cochlea; dendrite; excitability; outer hair cell; spiral ganglion**

Introduction

The mammalian cochlea contains inner hair cells (IHCs) and outer hair cells (OHCs), each signaling through a distinct population of spiral ganglion afferent neurons (Spoendlin, 1967, 1969; Kiang et al., 1982; Dannhof and Bruns, 1993; Hafidi, 1998; Nayagam et al., 2011). Myelinated type I spiral ganglion neurons comprise ~95% of the afferent neuron population and each receive input from a single active zone in a single IHC (Spoendlin, 1972; Perkins and Morest, 1975; Liberman, 1980). Type I afferents encode sound timing, intensity, and frequency (Young, 2010) at these specialized synapses that operate via multivesicular release from IHCs (Glowatzki and Fuchs, 2002; Nouvian et al., 2006; Goutman and Glowatzki, 2007). In contrast, the type II afferents receive synaptic inputs from multiple (~9; range, 1–31) OHCs (Perkins and Morest, 1975; Ginzberg and Morest, 1983; Brown, 1987; Simmons and Liberman, 1988; Berglund and Ryugo, 1991; Jagger and Housley, 2003; Weisz et al., 2012) and are thin and unmyelinated (Spoendlin, 1971; Romand and Romand, 1984; Romand and Romand, 1987; Brown, 1987; Brown et al., 1988). Excitatory synapses between OHCs and type II afferents also are glutamatergic (Weisz et al., 2009), but OHCs typically release single vesicles with low probability (Weisz et al., 2012). Thus, in contrast to large monophasic, multivesicular EPSPs that can evoke action potentials in type I afferents (Yi et al., 2010; Rutherford et al., 2012), summation of EPSPs from several OHCs would be required to reach threshold in the type II afferent.

In addition to benefiting from multivesicular release, the type I afferents are specialized for high-fidelity transmission by rapid postsynaptic responses (Grant et al., 2010; Rutherford et al., 2012) and a nearby spike initiation zone at the first heminode of the myelinated peripheral process ("dendrite"; Robertson, 1976; Hossain et al., 2005; McLean et al., 2009). In contrast, the type II spiral ganglion neurons have smaller, slower synaptic responses from widely distributed OHCs (Weisz et al., 2009, 2012). Thus, summation to spike threshold will depend on the length constant of the spiral dendrite and the distance to the heretofore unknown spike initiation site.

In the present work, dual-electrode recordings from the spiral process under the OHCs revealed length constants greater than the extent of the spiral dendrite. Dual recordings, as well as focal application of tetrodotoxin (TTX), demonstrated that action potentials initiated close to the spiral ganglion and then backpropagated into the spiral dendrite. A compartmental cable model replicated these experimental observations when a declining gradient of high-threshold voltage-gated sodium channels was incorporated into the spiral dendrite, consistent with previously reported immunolabeling (Hossain et al., 2005). Although im-

Received Aug. 9, 2013; revised Dec. 2, 2013; accepted Jan. 4, 2014.

Author contributions: C.J.C.W., E.G., and P.A.F. designed research; C.J.C.W. performed research; C.J.C.W. analyzed data; C.J.C.W., E.G., and P.A.F. wrote the paper.

This work was supported by NIDCD Grants R01 DC011741 (P.A.F., E.G.), P30 DC 005211 (to the Johns Hopkins Center for Hearing and Balance), T32 DC000023 (C.J.C.W.), and F31DC010948 (C.J.C.W.), and a grant from the Blaustein Pain Foundation of Johns Hopkins.

The authors declare no competing financial interests.

Correspondence should be addressed to Catherine J. C. Weisz, Department of Otolaryngology, University of Pittsburgh School of Medicine, Pittsburgh, PA 15261. E-mail: cchalen1@jhmi.edu.

DOI:10.1523/JNEUROSCI.3428-13.2014

 0270-6474/14/342365-09$15.00/0

portant for backpropagation, sodium channels had no effect on the high threshold for synaptic excitation. These results are consistent with the previously reported insensitivity to acoustic stimulation (Robertson, 1984; Brown, 1994; Robertson et al., 1999), suggesting that type II afferents may respond specifically to high-intensity sounds or serve as an integrator of acoustic information.

Materials and Methods

Sprague Dawley rat pups (Charles River Laboratories) of either sex of postnatal day 5 (P5) through P9 were anesthetized with isoflurane (Vedco) according to approved Johns Hopkins Institutional Animal Care and Use Committee guidelines. After ensuring deep anesthesia, each animal was decapitated, and the temporal bone containing auditory and vestibular peripheral organs was removed. Tissue was prepared as for previous experiments investigating both type I and type II spiral ganglion synaptic inputs (Glowatzki and Fuchs, 2002; Goutman and Glowatzki, 2007, 2011; Weisz et al., 2009, 2012; Grant et al., 2010; Yi et al., 2010). Specifically, the bone surrounding the cochlea was dissected away, and the apical turn of the cochlear spiral was severed at the modiolus. The stria vascularis and tectorial membrane were removed. The entire cochlear turn including the spiral ganglion and organ of Corti was mounted under an insect pin glued to a coverslip for electrophysiological experiments.

Standard gigaohm seal whole-cell patch-clamp techniques were used to record from dendrites of the type II afferent neurons under OHCs. Using differential interference contrast (DIC) optics, four to six OHCs (two per OHC row, beginning with row 3) were aspirated to expose the type II dendrites for recordings. Extracellular solution was perfused through the recording chamber at a rate of 2–3 ml/min. The solution contained the following (in mM): 5.8 potassium chloride, 155 sodium chloride, 1.3 calcium chloride, 0.9 magnesium chloride, 0.7 sodium phosphate, 5.6 glucose, and 10 HEPES, pH 7.4. The Intracellular solution contained the following (in mM): 20 potassium chloride, 110 potassium methanesulphonate, 0.1 calcium chloride, 5 magnesium chloride, 5 EGTA, 5 HEPES, 5 sodium-ATP, 0.3 sodium-GTP, and 5 sodium phosphocreatine, pH 7.2. Chemicals were purchased from Sigma-Aldrich. One millimeter borosilicate glass pipettes (WPI) were Sylgard coated (Corning) and fire polished to resistances of 6–10 MΩ. Recordings were performed using an Axopatch 200B or Multiclamp 700B amplifier, pClamp version 9.2, and a Digidata 1322A board (Molecular Devices). Data were sampled at 50 kHz and low-pass filtered at 10 kHz. Input resistances averaged at 192 ± 90 MΩ for type II afferents; series resistances were, on average, 17.4 ± 7.0 MΩ and were not corrected for. The membrane holding potential is given without a liquid junction potential correction of −9 mV.

For dual-electrode recordings, three holes were made through the epithelium by removal of four to six OHCs at intervals of ~100 μm. The first whole-cell recording was made in the center hole using a recording electrode with 10 μM green neuronal tracer (Alexa Fluor 488 hydrazide; Invitrogen) included in the pipette solution. After a few minutes to allow diffusion of the dye, the green fill was visualized under epifluorescence to localize the dendrite for recording with a second electrode, in whichever hole the fiber was most visible. The intracellular solution in the second electrode contained red neuronal tracer (Alexa Fluor 568 hydrazide; Invitrogen). The whole-cell recording configuration of the second electrode was achieved within 10 min of break-in of the first electrode.

For TTX puffing experiments, three action potentials were initiated by 10 ms depolarizations at intervals of 90 ms. The TTX puff was applied with a Picospritzer III (Parker Hannifin) using a glass pipette with a 2–3 μm diameter tip with a pressure of 5–7 psi. The puff began 10 ms before depolarization and continued through the current pulse for a total duration of 120 ms. For clarity, the voltage response to only the first current pulse is shown. Focal targeting of the puffer was confirmed visually by observing the slight movement of the fluorescently labeled dendrite in response to the puff. In separate experiments, the limited diffusion of the solution was confirmed by including the fluorescent tracer in the puff solution. To prevent diffusion of TTX from the targeted region of the neuron to other nontargeted regions, the puffer pipette was oriented to puff away from nontargeted regions, i.e., a pillar orientation for spiral segment targeting and a modiolar orientation for spiral ganglion and radial segment targeting.

Voltage recordings were analyzed in Clampfit 9.2 (Molecular Devices), with additional analysis of EPSPs performed using MiniAnalysis software (Synaptosoft). The EPSP selection criterion was five times the root mean square of the noise, and then individual EPSPs were accepted or rejected by eye based upon characteristic waveform. The length constant was calculated by plotting the normalized amplitudes of steady-state voltage changes in response to current injection on a semilog plot and then extrapolating a line fit to the data to e^{-1}, the x-axis value of which is the length constant. Figures were prepared in Origin 8.0 (Origin Labs) and Illustrator CS2 (Adobe). Statistical analysis was performed with Origin 8.0. All data are presented as mean ± SD.

Cochlear explants were viewed for electrophysiological experiments under an Examiner D1 microscope (Zeiss) using DIC optics using a 40× water-immersion objective and a camera with contrast enhancement (Hamamatsu). Fluorescent images of dye-filled neurons were collected using an upright fluorescent microscope (Leica). Tiled images were traced in Photoshop (Adobe).

A neuron from which dual-electrode recordings were achieved and that had a completely filled dendritic arbor was used for mathematical modeling (NEURON software version 7.2; Carnevale and Hines, 2006). The modeled neuron had a spiral dendritic segment of 380 μm in length, with 14 branches ranging from 1 to 5 μm in length. The branches were only found in the terminal third of the dendrite. The neuronal tracer did not fully fill the radial portion of the dendrites or the soma, so an estimated radial segment length of 350 μm was used, and a somatic size of length 15 μm and diameter 12 μm (Romand and Romand, 1987). Radial and spiral dendrite diameters were 1 μm, and branch diameters were 0.6 μm. On each side of the soma, a segment of 6.5 μm in length was added to allow insertion of additional sodium channels in these distinct regions to replicate published immunolabel results and a compartmental model (Hossain et al., 2005). This radial segment was 0.9 μm in diameter, whereas the central segment adjacent to the soma was 1.2 μm in diameter. An axon of length 100 μm and diameter 1.0 μm was added. The neuronal segments were automatically divided into 0.1 μm compartments using the "d_lambda" function of NEURON. The model used a uniform access resistance of 250 Ω cm and a membrane capacitance of 1 μF/cm^2. The biophysical parameters were adjusted to mimic the conditions in which current injection or synaptic conductance in the spiral portion of the dendrites initiated action potentials that occurred first in the soma, followed by a spike in the peripheral dendrites. All compartments had a baseline membrane potential of −65 mV, except the soma, which had a membrane potential of −67 mV. The default Hodgkin–Huxley channels were inserted into some compartments at the following densities (in S/cm^2): sodium channels, 0.11 (soma), 0.1 (radial dendrite adjacent to soma), 0.08 (radial segment), 0.1 (axon); potassium channels, 0.007 (soma, radial dendrite adjacent to soma, radial segment, axon); leak potassium channels, 0.003 (soma, radial dendrite adjacent to soma, radial segment, axon). Additional selected channel types included an A-type potassium channel (Hoffman et al., 1997; 0.04 S/cm^2, spiral dendrites; 0.012 S/cm^2, soma) as well as a high-threshold sodium channel (Mainen and Sejnowski, 1996; 0.012 S/cm^2, spiral dendrites) with a gradient of −0.003. The properties of these channels were constructed using the "channel builder" function of NEURON. The model recapitulated the action potential initiation zone and backpropagation of the action potentials into the dendrites, but with a slightly lower threshold (~3 mV) than was measured during the experiments.

Results

Length constant measured by current injection

The cochlear apical turn of P5–P9 rats was mounted flat under an insect pin glued to a coverslip for whole-cell electrophysiological recordings. In this preparation, the cell bodies of spiral ganglion neurons remain intact in the modiolus, as well as

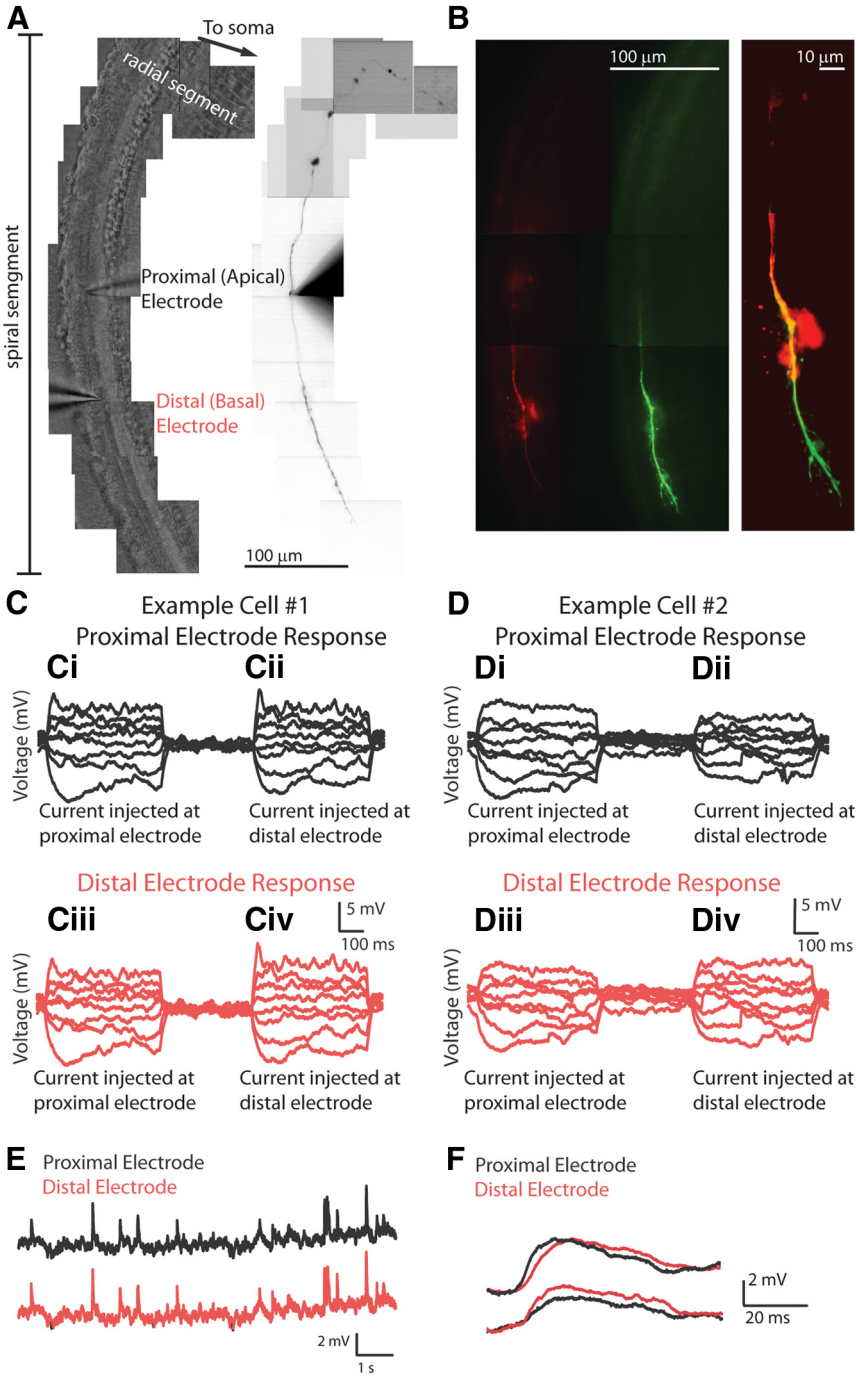

Figure 1. Dual recordings from a type II afferent dendrite. ***A***, Left, Tiled DIC image of the organ of Corti showing the placement of two recording electrodes, both in the spiral segment of dendrite, spaced ~100 μm apart (average, 101.2 ± 7.6 μm). Right, Same field of view; fluorescent view of neuron. Alexa Fluor 488 hydrazide tracer signal is visible in the proximal electrode solution and filled type II dendrite. The second electrode contains Alexa Fluor 568 hydrazide and is not visible. ***B***, Left, Both the Alexa Fluor 488 hydrazide (green) and the Alexa Fluor 568 hydrazide (red) tracers are visible in the same type II afferent dendrite, confirming a dual recording. A more complete fill is visible for the green tracer, from the electrode placed first. Right, Merged and enlarged image of green and red filled fibers (contrast enhanced). ***C***, ***D***, Passive flow of current in a single dendrite measured at two electrodes in two exemplar neurons. ***Ci***, ***Cii***, Voltage recording from the electrode proximal to the cell soma. ***Ci***, Voltage response to current injected at this electrode. ***Cii***, Voltage response to current injected at the other, distal electrode, 98 μm distant. ***Ciii***, ***Civ***, Voltage recording from the electrode distal to the cell soma. ***Ciii***, Voltage response to current injection at the other electrode; passive propagation. ***Civ***, Voltage response to current injection at this electrode. ***D***, Same experimental design as in ***C*** for a different neuron (electrode spacing, 94 μm). ***E***, Simultaneous measurement of EPSPs from two electrodes recording from the same dendrite. Top (black), Voltage recording from the proximal electrode showing EPSPs induced by local application of 40 mM KCl solution via a large-bore gravity-driven pipette. Bottom (red), Simultaneous voltage recording from the distal electrode. The patterns of EPSPs are the same at both electrodes. ***F***, Exemplar EPSPs recorded simultaneously at the proximal (black) and distal (red) electrodes. Top, EPSP peaking first at the proximal electrode. Bottom, EPSP peaking first at the distal electrode.

their peripheral connections to presynaptic hair cells in the organ of Corti. Type II afferents project radially, across the tunnel of Corti (radial segment), then turn toward the cochlear base to contact numerous OHCs (spiral segment). Thus, more basal portions of the fiber are further (distal) from the soma than apical (proximal) portions. In all experiments, dye filling through the recording electrode confirmed that the entire spiral portion under OHCs remained intact. Four to six OHC were removed by aspiration to expose the type II afferent dendrites spiraling beneath them. For experiments in which the same dendrite was patched with two different recording electrodes, three holes were made at 100 μm intervals. A recording electrode containing a green fluorescent tracer (Alexa Fluor 488 hydrazide) was used to perform whole-cell recordings from a type II afferent directly under the OHCs. Fluorescence imaging of the Alexa Fluor dye was used to locate the same fiber 100 μm away (average, 101.2 ± 7.6 μm; $n = 5$) in either the basal (distal) or apical (proximal) direction along the spiral segment, wherever it was most visible under epifluorescent illumination. A second intracellular recording was obtained with an electrode containing red fluorescent neuronal tracer (Alexa Fluor 568 hydrazide; Fig. 1*A*). The diffusion of both the green and red fluorescent dyes provided confirmation that both electrodes were recording from the same type II fiber, although the two dyes filled the dendrite to different degrees depending on the order of electrode placement and the length of time that each seal was held (Fig. 1*B*).

In the current-clamp recording configuration, 10 pA hyperpolarizing and depolarizing steps were injected sequentially at each electrode while recording simultaneously from both (Fig. 1*C*,*D*). The length constant of the dendrite was computed from the decrease in amplitude of the steady-state voltage response from the active (current injection) to the passive electrode. In some cases, virtually no decrement in voltage change was observed between electrodes (Fig. 1*C*), whereas in other fibers a difference between electrodes was more readily apparent (Fig. 1*D*). In five such experiments, the length constant based on these dual recordings was 1189.6 ± 1011.4 μm (range, 362 to 2855 μm; $n = 5$). Average length constant measurements were used to derive specific membrane resistance (24.7 kΩ cm^2)

and axial resistance (43.6 Ω cm). Neither the choice of electrode for current injection nor the order of placement of the electrodes along the dendrite affected the measurements.

Spatial spread of synaptic inputs

Synaptic events were infrequent in baseline recording conditions (Weisz et al., 2009). Therefore, in three longer-lasting dual recording experiments, EPSPs were evoked by 40 mM potassium solution perfused onto the tissue via a large-bore pipette to depolarize presynaptic OHCs and induce neurotransmitter release. Nearly identical patterns of potassium-evoked EPSPs were measured at the two electrodes, with only small differences in rise time and amplitude (Fig. 1*E*,*F*). In all three recordings, EPSPs could be measured first, and with faster rise times and larger amplitudes, at either electrode (Fig. 1*F*; 78, 82, and 38% measured first at the distalmost electrode in three recordings, respectively). This indicates that the synaptic inputs originated at multiple points along the dendrite, and that the two electrodes were placed within the synaptic field.

Active enhancement of synaptic inputs

EPSPs recorded in current clamp in both normal (5.8 mM) and high (40 mM) extracellular potassium (Weisz et al., 2009) were reanalyzed to measure kinetics. The EPSPs were usually monophasic, with an average amplitude of 3.8 ± 2.0 mV and a rise time of 3.0 ± 1.1 ms (Fig. 2*A*). However, in two of eight recordings, an additional population of EPSPs with larger amplitudes and faster kinetics was apparent (Fig. 2*B*). A histogram of rise times (0.2 ms bins) from cells in which these faster events were observed was fit with two Gaussians centered at 1.42 and 2.72 ms (Fig. 2*D*). The amplitude histogram of EPSPs in a cell without larger, fast events was fit with a single Gaussian centered at 2.33 ms (Fig. 2*C*). Plots of the rise time by amplitude show that the fastest EPSPs had the largest amplitudes (Fig. 2*F*). These larger, faster EPSPs may reflect the contribution of voltage-gated conductances. Indeed, compartmental modeling to follow suggests that voltage-gated sodium channels could be present in the extended spiral dendrite and so contribute to the large, fast EPSPs.

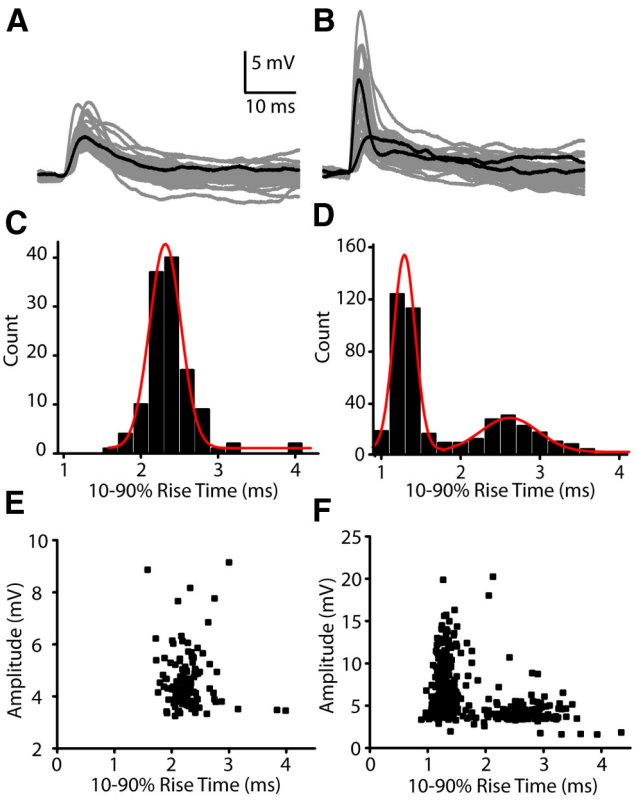

Figure 2. Two subsets of EPSPs in type II afferent neurons. ***A***, Fifty overlaid EPSP traces recorded from a representative type II neuron dendrite. ***B***, Fifty overlaid traces from a different neuron with a mixed population containing some EPSPs with amplitudes and kinetics similar to those in ***A***, and an additional population of larger EPSPs with faster rise times. ***C***, Frequency histogram of EPSP rise times from the same cell as in ***A***. A Gaussian fit to the data has a center at 2.33 ms. ***D***, Frequency histogram of EPSP rise times from the same cell as in ***B***. Data can be fit with two Gaussian curves, with centers at 1.29 and 2.62 ms. ***E***, Plot of amplitude by rise times for EPSPs from same cell as in ***A***, ***C***. ***F***, Plot of amplitude by rise times for EPSPs from same cell as in ***B***, ***D***.

Site of action potential initiation

Length constant measurements suggest that synaptic inputs should be able to summate within the type II dendrite and trigger an action potential, depending on the distance to the site of initiation. Dual recordings during activation of action potentials indicated that these initiated proximal to both recording sites (Fig. 3). Regardless of which electrode was used to initiate the spike, it always occurred first at the proximal electrode, closer to the cell soma, where it also had a larger amplitude and faster waveform (Fig. 3*C*,*D*; $n = 5$). This also was independent of whether the proximal or distal electrode was positioned first. These observations indicate that the action potential is initiated central to both electrodes and then backpropagates into the spiral segment under the OHCs. Thus, synaptic depolarization of the type II fiber must be large enough to reach this centrally located initiation site. The larger, faster action potentials recorded at the proximal electrode had an average depolarization of 80.7 ± 12.9 mV from a baseline of −61.8 ± 3.8 mV, with a rise time of 1.2 ± 0.3 ms, and a full-width at half-maximum (FWHM) of 2.3 ± 0.8 ms. At the distal electrode, the depolarization averaged 62.2 ± 13.3 mV from a baseline of −58.6 ± 6.4 mV, a rise time of 1.5 ± 0.4 ms, and a FWHM of 4.8 ± 2.0 ms. The action potential conduction velocity was 0.31 ± 0.34 m/s ($n = 12$ proximal electrode current injection, 10 distal electrode current injection, 5 experiments). Action potentials also were recorded first at the proximal electrode during bath application of high-potassium solution ($n = 3$). Therefore even when the depolarization was distributed due to the widespread application of high-potassium solution (or distributed synaptic inputs), the action potential initiation zone was still central to the electrode recording sites.

Tetrodotoxin block of action potentials

Focal application of TTX was used to further probe the action potential initiation zone of the type II afferent. From a single recording electrode in the spiral portion of type II dendrites under OHCs (Fig. 4*B*,*D*), depolarizing pulses (10 ms duration, 250 pA) were injected to elicit a spike (Fig. 4*Ai*,*Ci*). A neuronal tracer was included in the pipette solution to visualize the fiber's trajectory. A puff pipette was used to focally apply 5 μM TTX to different regions of the dendrites. First, TTX was targeted to the spiral segment of the dendrites ($n = 2$) through an opening (~15 μm diameter) in the epithelium made by removing two to four OHCs. Multiple holes were made at 100 μm intervals along the entire length of the selected dendrite. Focal application of TTX to the spiral portion of the dendrites blocked the action potential, leaving only the small local voltage change induced by the current pulse (Fig. 4*Aii*). Increasing the pulse intensity to 500 pA produced a voltage change with an inflected rising phase (Fig. 4*Aiii*, arrow) and more rapid repolarization than the response to 250

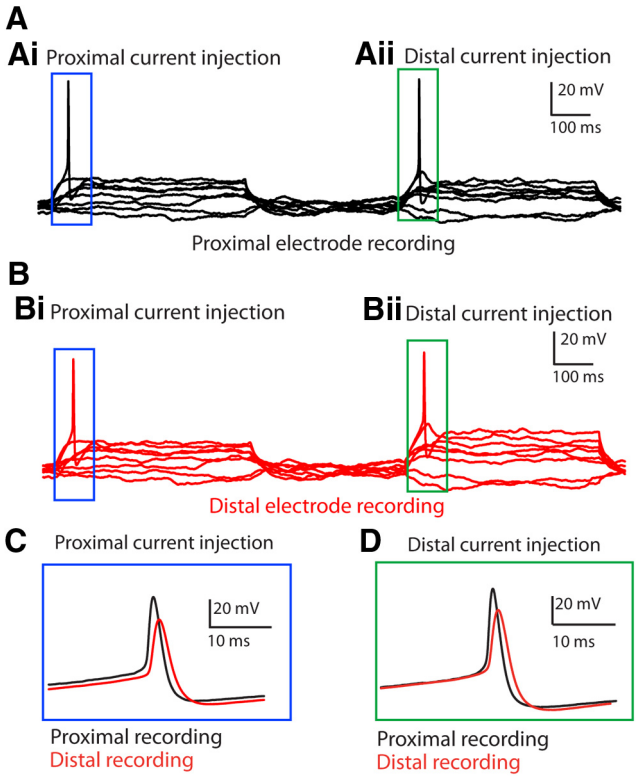

Figure 3. Dual-electrode recordings of action potentials. ***A***, Recording from proximal electrode during sequential current injection (steps increasing by 10 pA from −30 to +70 pA; select traces are shown for clarity) into proximal (***Ai***) and distal (***Aii***) electrodes. Electrodes are spaced 110 μm apart. Thus, the proximal electrode was "active," i.e., current was injected into the recording electrode on the left half of the trace. ***B***, Simultaneous distal electrode recording during sequential current injection protocol as in ***A***. Thus, the distal electrode was passive on the left side of the trace (***Bi***), but "active" on the right side (***Bii***). ***C***, Magnified records of action potentials in proximal (black) and distal (red) electrodes during proximal current injection. The blue box is positioned similarly to those in ***Ai***, ***Bi*** (not to scale). ***D***, Magnified records of action potentials in proximal (black) and distal (red) electrodes during distal current injection. The green box is positioned similarly to those in ***Aii***, ***Bii*** (not to scale). Note that the proximal action potential was larger and faster in both conditions.

pA current injection blocked by TTX, suggestive of initiation of an active process. Application of TTX anywhere along the spiral portion of the dendrite failed to block completely these smaller active responses. The action potential threshold and waveform recovered to initial values upon washout of TTX (Fig. 4*Av*).

In five experiments, the puffer pipette was positioned to apply TTX close to the neuronal cell body in the spiral ganglion. The tissue was oriented so that the puff was directed toward the spiral ganglion, and the puff direction was confirmed in experiments in which a red dye was included in the puffer pipette solution. The neuronal tracer dye fill allowed localization of the radial portion of the dendrite, but the cell soma was never visible during the experiment. Therefore, blind puffing of TTX to the spiral ganglion was attempted. In one of five experiments, action potentials elicited by current injection in the spiral portion of the dendrite were blocked when TTX was focally applied to a restricted region above the neuron cell bodies. In this experiment, TTX puff application to regions surrounding the presumed cell body in the spiral ganglion, averaging 37.7 ± 9.7 μm distant in any direction along the spiral ganglion surface, failed to block action potentials. In four other experiments, the TTX puff targeted to the spiral ganglion failed to block action potentials. Therefore, the TTX puff pipette was driven through the tissue and positioned along the radial portion of the dendrite (localized using the dye fill) about 30 μm from the border with the spiral ganglion. Focal TTX application to the radial segment of the dendrite also blocked action potential initiation (Fig. 4*Cii*). In contrast to application of TTX on the spiral dendrite under OHCs, the largest current injections failed to overcome TTX block of the radial dendrite near the spiral ganglion (Fig. 4*Ciii*,*Civ*). The depolarization in TTX represents the direct, passive response to the current injection. The missing inflection in this depolarization points to the fact that no active process was activated, as it had been for the recording in the control (Fig. 4*A*, arrow). Additionally, the increased amplitude of the responses to current injection when action potentials are blocked by TTX application to the radial segment suggests an increased resistance due to the loss of the shunting effect of the action potential. After TTX was washed from the preparation, action potential threshold and waveform recovered to initial values (Fig. 4*Cv*).

Type II neuron compartmental model

A compartmental cable model of the type II afferent dendrite was constructed (NEURON software) based on these recordings (see Materials and Methods). Dye filling provided images of type II fibers for morphological measurements. A type II neuron with representative morphology and electrical properties was selected for the modeling (Figs. 1*B* 5*D*, line illustration).

Voltage-gated sodium and potassium channel densities were adjusted in the model to replicate experimental observations of action potential propagation. The neuronal soma and a short, proximal radial segment were given a larger sodium conductance, consistent with the central locus of spike initiation and the efficacy of TTX blockade in those regions. To obtain action potential initiation as observed in the radial dendrite, it proved necessary to add a lower level of sodium conductance to the remainder of the radial dendrite. Finally, in addition to standard Hodgkin–Huxley sodium and potassium conductances, an "A-type" potassium channel was placed in the spiral dendrites and soma, and high-threshold sodium channels replaced default sodium currents in the spiral dendrites in a gradient with the highest sodium conductance closest to the soma. These proved necessary to obtain the observed relationship between action potential threshold and site of initiation. The magnitude of conductances used in the model was determined operationally, since each ionic component has not been characterized experimentally. However, the intent of the model was to replicate experimentally observed action potential threshold and conduction, and from that to determine the threshold for synaptic activation. Simulated current injection (50 pA, 100 ms) into the spiral portion of the model dendrite evoked an action potential that originated in the soma and then backpropagated into the dendrite (Fig. 5*A*), as observed experimentally. Reducing sodium channel density in the spiral portion of the dendrite reduced the amplitude of the backpropagating action potential, without affecting the somatic spike (Fig. 5*B*). Independent of the exact complement of conductances, it is clear that action potentials observed in the spiral dendrite of the type II afferent could only occur if voltage-gated sodium channels were expressed there, confirming previous conclusions based on immunolabeling experiments (Hossain et al., 2005). This experiment also illustrates that peripherally located sodium channels, although supporting backpropagating action potentials, have no effect on the threshold for the peripheral initiation of the action potential. When current injection was lowered to that required for spike initiation (33 pA), reduction of peripheral sodium channel density (from 0.012 to 0.011 S/cm^2) did not prevent central spike initiation. Further reduction in sodium channel density diminished the backpropagating action potential

amplitude, as seen for suprathreshold stimulation (Fig. 5*B*). Thus, although voltage-gated sodium channels may give rise to larger, faster EPSPs (Fig. 2*B*), this is unlikely to alter the threshold for synaptic excitation. Synaptic inputs were distributed randomly to peripheral branchlets of the model. These were set equal to the average synaptic conductance change observed in recordings, 0.13 nS, yielding a voltage change of 3.75 mV, matched to the observed amplitude and waveform at the site of recording (decay time of 6.8 ± 4.3 ms calculated from previously published data; $n = 1709$ EPSPs, eight recordings; Weisz et al., 2009). The action potential threshold was reached when six synaptic events occurred simultaneously (Fig. 5*C*). Given the low average release probability of OHCs, 0.26, this result requires that 24 OHCs be connected to the model type II afferent, within the range of the estimated number of functional synapses onto a type II afferent (Weisz et al., 2012). Synaptic inputs could be temporally spread up to 7 ms from the onset of the first EPSP and still exceed the threshold; additional spread resulted in subthreshold EPSPs.

Discussion

Synaptic inputs from OHCs onto type II afferent neurons are less frequent and weaker than IHC synapses onto type I afferent neurons, raising the question of what role type II afferents might play in acoustic signaling. Previous estimates suggest that suprathreshold excitation would require summation of inputs from the entire pool of presynaptic OHCs, spread hundreds of micrometers along the cochlear spiral (Weisz et al., 2009, 2012). The efficacy of that summation will depend on the electrical membrane properties of the type II afferent. Here we show that type II neurons have passive length constants longer than their spiral process, enabling summation from all presynaptic OHCs. In addition, dual-electrode recordings, focal application of tetrodotoxin, and a compartmental conduction model support the hypothesis that a proximal-to-distal declining gradient of high-threshold voltage-gated sodium channels (Hossain et al., 2005) enable backpropagation of action potentials into the spiral dendrite.

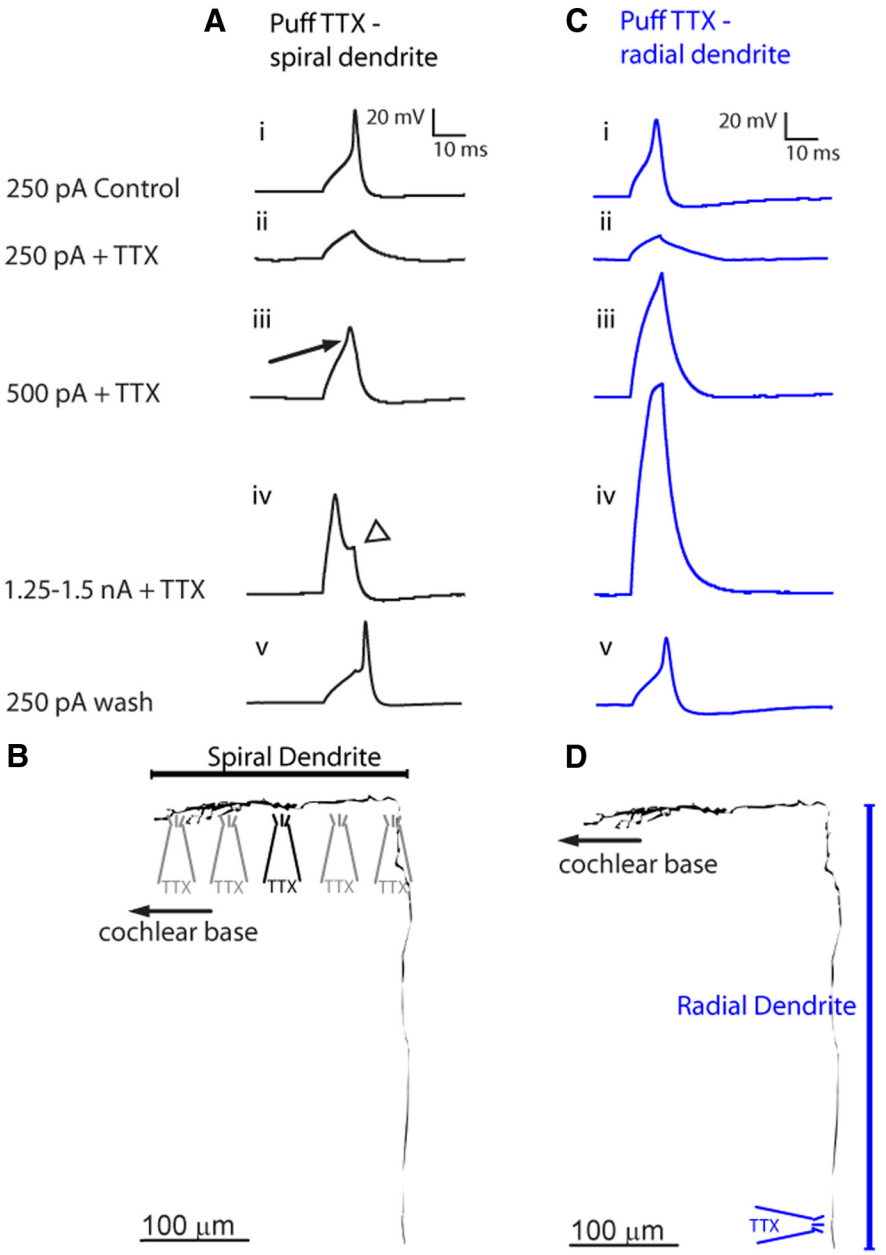

Figure 4. Focal application of TTX localizes the action potential (AP) initiation zone. ***A***, APs initiated by 10 ms depolarizing current pulses from a single recording electrode located in the spiral portion of the dendrite. ***Ai***, Control AP initiated by a 250 pA pulse. ***Aii***, AP blocked by a focal "puff" of TTX along spiral portion of dendrite ~100 μm from the recording site. The local voltage change remains. ***Aiii***, A stronger depolarizing pulse of 500 pA overcomes the TTX block, and the inflected action potential waveform is recorded (arrow). ***Aiv***, A larger and faster AP waveform elicited by a 1.25 nA depolarizing pulse during the TTX puff, at the dendrite "turn" toward base of cochlea. The portion of local voltage change induced by a 10 ms current step is visible (arrowhead). ***Av***, AP waveform after wash of TTX, 250 pA current pulse. ***B***, Representative trace of a filled type II afferent dendrite. The spiral segment is indicated. The orientation of the TTX puffer pipette for experiments shown in ***A*** is indicated. Gray TTX puffers indicate that multiple puffer positions along the spiral dendrite were tested in the same experiment, with wash of TTX between tests (4–7 locations tested per experiment), with indistinguishable results. ***C***, APs initiated in same manner as in ***A*** in a different neuron. ***Ci***, Control AP initiated by 250 pA current pulse. ***Cii***, AP blocked by focal "puff" of TTX onto the radial portion of the dendrite, 30 μm from spiral ganglion border. ***Ciii***, ***Civ***, TTX puff prevents AP induced by depolarizing pulses of 500 pA (***Ciii***) or 1.5 nA (***Civ***). ***Cv***, AP initiated by 10 ms, 250 pA current pulse after wash of TTX. ***D***, Representative trace of a filled type II afferent dendrite. The radial segment is indicated. The orientation of the TTX puffer pipette for experiments shown in ***C*** is indicated.

Current spread in the spiral process of type II neurons

In a previous study (Weisz et al., 2012), EPSCs were initiated from OHCs at different distances from the recording electrode to estimate length constants greater than one millimeter. In the present work, current injection and voltage responses at two intracellular electrodes separated by ~100 μm provided a direct length constant measure of ~1200 μm. Length constant measurements and the fiber diameter were used to derive a specific membrane resistance of 20 to 40 k Ω cm^2, in the range of those

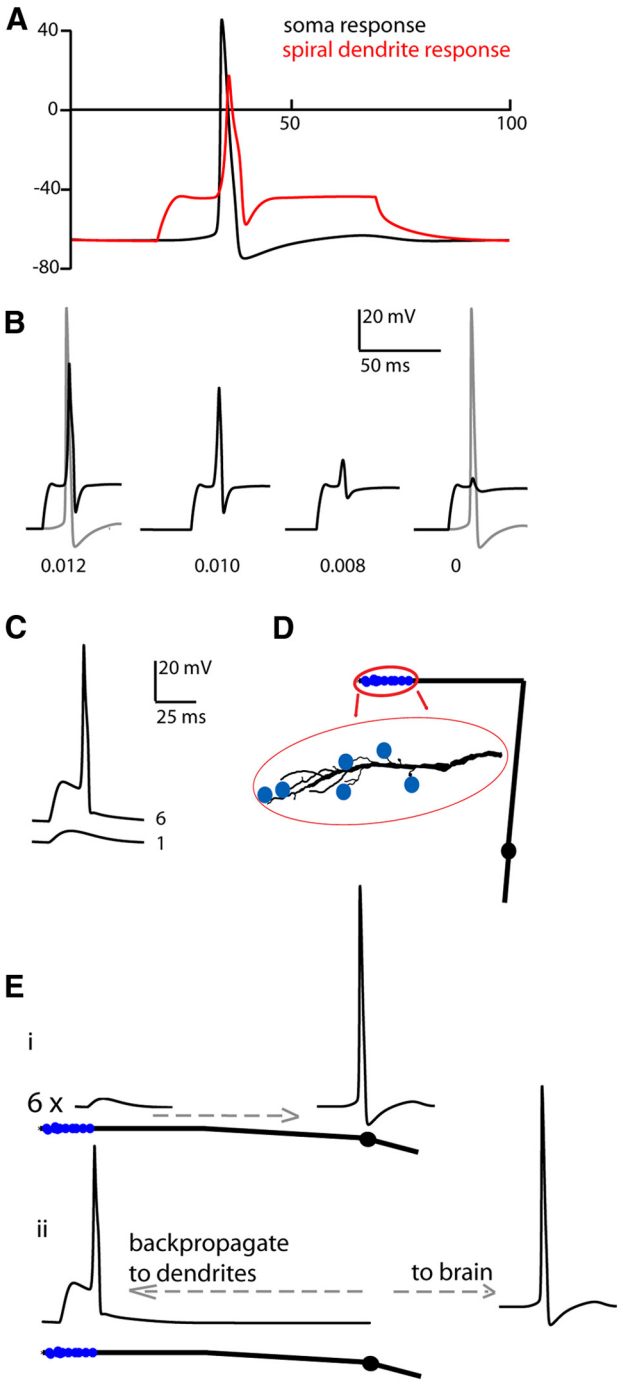

Figure 5. Computational model of action potential (AP) initiation in a type II afferent dendrite. ***A***, Voltage response to simulated current injection in the spiral segment of dendrites (50 ms duration, 50 pA). Black trace, AP waveform in somatic compartment. Red trace, Action potential waveform in spiral dendritic segment. ***B***, Black traces, AP response of spiral dendritic segment to same stimulus as in ***A***. Gray, Response in somatic compartment. Decreased current density of sodium channels (numbers listed below each set of traces in siemens per square centimeter) reduces the amplitude of the spiral compartment backpropagating AP, but does not affect the somatic action potential. ***C***, Simulated synaptic currents of amplitude 3.75 mV injected at the branches of the model neuron. Bottom trace, Response to a single synaptic input. Top trace, Response to six simultaneous synaptic inputs, with resulting AP. ***D***, Line illustration of the modeled neuron. Blue filled circles indicate the location of simulated synaptic inputs added in ***C***. Enlarged is a tracing of the actual filled neuron upon which morphological and biophysical parameters were based (the same neuron as in Fig. 1*B*). ***E***, Diagram of action potential generation and propagation in a type II neuron. A linearized diagram of the neuron from ***D*** is shown. ***Ei***, The summed depolarization from six synaptic inputs propagates to the perisomatic region where an action potential is initiated. ***Eii***, The action potential both propagates centrally to the brain as well as backpropagates into the dendrites.

reported for olfactory neurons (100 k Ω cm^2, Pongracz et al., 1991) and cortical pyramidal neurons (20 k Ω cm^2; Kabaso et al., 2009). As expected for an unmyelinated fiber, the action potential conduction velocity was slow (~0.31 m/s). However, this is slower than reported for other unmyelinated fibers (0.66–7 m/s; Van Hees and Gybels, 1972; Yoshimura and Jessell, 1989; Slugg et al., 2000; Carr et al., 2003), in part because the recordings performed here were at room (22–24°C) instead of body (35–37°C) temperature. In addition, action potentials are smaller and broader in the more distal spiral dendrite, consistent with the declining gradient of excitability incorporated into the compartmental model and contributing to an apparent slowing of conduction velocity.

A concern for any study of membrane resistance is that the recording electrodes might create a leak conductance, which would be expected to reduce the measured length constant. Presumably this effect would be exacerbated with two intracellular electrodes, as used here. However, the present length constants obtained with two electrodes were equivalent to those derived previously using a single electrode (Weisz et al. 2012), suggesting at least that an additional patch pipette did not produce a significant additional shunt. Also, neither the sequence of electrode placement nor their relative positions correlated with amplitude measurements, arguing against systematic shunting of input resistance. Regardless of experimental shunting, the reported length constants support the conclusion that synaptic inputs can sum effectively throughout the spiral process of the type II neuron.

Summation and conduction in the spiral dendrite

The action potential threshold in the spiral dendrite is ~25 mV positive to rest. This relatively high voltage threshold, as well as all-or-none "action currents" observed in voltage clamp (Weisz et al., 2009), suggest that the spike trigger zone may be some distance from the recording site in the spiral dendrite. Consistent with that suggestion, action potentials always propagated from the proximal to the distal electrode in dual recordings, and so must initiate somewhere central to the recording sites in the spiral process, rather than nearer the synaptic input zone. Likewise, TTX completely blocked active responses even with increased stimulus intensity only when applied to the radial process near the spiral ganglion. Nonetheless, overshooting action potentials were commonly observed in the spiral process, and immunolabel for $Na_v1.6$ extends throughout the peripheral arbor (Hossain et al., 2005).

Sodium channel-dependent backpropagation of action potentials into dendrites has been demonstrated in brain slice experiments in the neocortex (Stuart and Sakmann, 1994), CA1 hippocampal pyramidal cells (Spruston et al., 1995; Stuart et al., 1997), and spinal cord motoneurons (Larkum et al., 1996). Neuronal models have also implicated sodium conductances in action potential backpropagation (Rapp et al., 1996; Colbert and Pan, 2002). A-type potassium channels may also play a role in the backpropagation of action potentials into dendrites with implications for plasticity. Dendritic A-type potassium channel density has been shown to limit the amplitude of backpropagating action potentials (Hoffman et al., 1997; Johnston et al., 2000). Furthermore, A-type potassium currents have been proposed to play a role in dendritic plasticity in conditions in which EPSPs can inactivate A-type potassium currents, increasing the amplitude of subsequent EPSPs or backpropagating sodium spikes (Pan and Colbert, 2001; Makara et al., 2009).

Thus, experimental observation and the compartmental model both support the hypothesis that the extended spiral den-

drite of the type II afferent is essentially an integrator of inputs for a central spike initiation zone, and can therefore be classified as a dendrite. However, ionic mechanisms are present in the type II dendrites that may have a role in the plasticity of inputs from OHCs. An important implication is that the small synaptic inputs arising from OHC transmitter release will sum approximately linearly, as indeed seen in the model. Consequently, six synchronous synaptic inputs were required to generate spikes in the model neuron. Given their average low release probability, this would mean that maximal stimulation of 24 presynaptic OHCs is required for functional central signaling by the model type II neuron. This is within the range of connected OHCs estimated in previous studies and is consistent with the general conclusion that type II neurons would be very insensitive to acoustic input.

Implications of the compartmental model for type II neuronal function

The neuronal model (NEURON version 7.2 software; Carnevale and Hines, 2006) was constructed using the morphological and electrical properties of a representative neuron from which dual recordings were performed. Default Hodgkin–Huxley sodium and potassium conductances were used in the soma, axon, and radial portion of the dendrites (see Materials and Methods). To reproduce experimental observations of spike initiation in the soma or adjacent radial dendrite, followed by action potential backpropagation into the peripheral spiral dendrites, channels that have been described and used previously in models of dendritic excitability were added in the spiral dendrites, specifically an A-type potassium channel (Hoffman et al., 1997) and a high-threshold sodium channel (Mainen and Sejnowski, 1996). The sodium channels were placed in the spiral dendrites with a decreasing gradient from the proximal to the distal portions. The functional contribution of peripheral sodium channels was examined further using the type II compartmental model, which showed that these were required for backpropagation into the spiral process, but did not contribute to setting the action potential threshold. These effects were produced in the model by populating the peripheral process with a lower density of sodium channels whose voltage sensitivity was more positive than those in the soma and initial segment. A declining gradient of sodium channels into the terminal dendritic arbor accords with the experimental observation of smaller, slower action potentials consistently found in the more distal recording electrode. A-type potassium conductances were shown to be a prominent feature of type II neurons studied in cochlear slice preparations (Jagger and Housley, 2003). The exact level of channel expression in the type II neuron is not known. On the other hand, measurements of passive membrane properties also vary by more than a factor of 2. Thus, whereas qualitative properties of the chosen ion channels (relative activation range, kinetics, inactivation) are assumed, the effect of channel densities will depend strongly on the native membrane resistance of the fiber, as well as assumptions regarding OHC excitability. It is possible that OHC transmitter release is substantially different *in vivo* than observed in the *ex vivo* cochlear preparations. For example, it has been reported that OHC resting membrane potential may be near −40 mV due to the high open probability of mechanotransducer channels in low-calcium endolymph (Johnson et al., 2011). Transmitter release by hair cell ribbons shows a form of facilitation (Goutman and Glowatzki, 2011) that may be present in OHCs with less negative resting membrane potentials. All of these factors would go toward improving the synaptic transfer function from OHCs to type II afferents. Nonetheless, even so improved, acoustic signaling by the type II afferent would remain limited to strong OHC stimulation.

References

Berglund AM, Ryugo DK (1991) Neurofilament antibodies and spiral ganglion neurons of the mammalian cochlea. J Comp Neurol 306:393–408. CrossRef Medline

Brown MC (1987) Morphology of labeled afferent fibers in the guinea pig cochlea. J Comp Neurol 260:591–604. CrossRef Medline

Brown MC (1994) Antidromic responses of single units from the spiral ganglion. J Neurophysiol 71:1835–1847. Medline

Brown MC, Berglund AM, Kiang NY, Ryugo DK (1988) Central trajectories of type II spiral ganglion neurons. J Comp Neurol 278:581–590. CrossRef Medline

Carnevale NT, Hines ML (2006) The neuron book. Cambridge, UK: Cambridge UP.

Carr RW, Pianova S, Fernandez J, Fallon JB, Belmonte C, Brock JA (2003) Effects of heating and cooling on nerve terminal impulses recorded from cold-sensitive receptors in the guinea-pig cornea. J Gen Physiol 121:427–439. CrossRef Medline

Colbert CM, Pan E (2002) Ion channel properties underlying axonal action potential initiation in pyramidal neurons. Nat Neurosci 5:533–538. CrossRef Medline

Dannhof BJ, Bruns V (1993) The innervation of the organ of Corti in the rat. Hear Res 66:8–22. CrossRef Medline

Ginzberg RD, Morest DK (1983) A study of cochlear innervation in the young cat with the Golgi method. Hear Res 10:227–246. CrossRef Medline

Glowatzki E, Fuchs PA (2002) Transmitter release at the hair cell ribbon synapse. Nat Neurosci 5:147–154. CrossRef Medline

Goutman JD, Glowatzki E (2007) Time course and calcium dependence of transmitter release at a single ribbon synapse. Proc Natl Acad Sci U S A 104:16341–16346. CrossRef Medline

Goutman JD, Glowatzki E (2011) Short-term facilitation modulates size and timing of the synaptic response at the inner hair cell ribbon synapse. J Neurosci 31:7974–7981. CrossRef Medline

Grant L, Yi E, Glowatzki E (2010) Two modes of release shape the postsynaptic response at the inner hair cell ribbon synapse. J Neurosci 30:4210–4220. CrossRef Medline

Hafidi A (1998) Peripherin-like immunoreactivity in type II spiral ganglion cell body and projections. Brain Res 805:181–190. CrossRef Medline

Hoffman DA, Magee JC, Colbert CM, Johnston D (1997) K+ channel regulation of signal propagation in dendrites of hippocampal pyramidal neurons. Nature 387:869–875. CrossRef Medline

Hossain WA, Antic SD, Yang Y, Rasband MN, Morest DK (2005) Where is the spike generator of the cochlear nerve? Voltage-gated sodium channels in the mouse cochlea. J Neurosci 25:6857–6868. CrossRef Medline

Jagger DJ, Housley GD (2003) Membrane properties of type II spiral ganglion neurones identified in a neonatal rat cochlear slice. J Physiol 552:525–533. CrossRef Medline

Johnson SL, Beurg M, Marcotti W, Fettiplace R (2011) Prestin-driven cochlear amplification is not limited by the outer hair cell membrane time constant. Neuron 70:1143–1154. CrossRef Medline

Johnston D, Hoffman DA, Magee JC, Poolos NP, Watanabe S, Colbert CM, Migliore M (2000) Dendritic potassium channels in hippocampal pyramidal neurons. J Physiol 525:75–81. CrossRef Medline

Kabaso D, Coskren PJ, Henry BI, Hof PR, Wearne SL (2009) The electrotonic structure of pyramidal neurons contributing to prefrontal cortical circuits in macaque monkeys is significantly altered in aging. Cereb Cortex 19:2248–2268. CrossRef Medline

Kiang NY, Rho JM, Northrop CC, Liberman MC, Ryugo DK (1982) Hair-cell innervation by spiral ganglion cells in adult cats. Science 217:175–177. CrossRef Medline

Larkum ME, Rioult MG, Lüscher HR (1996) Propagation of action potentials in the dendrites of neurons from rat spinal cord slice cultures. J Neurophysiol 75:154–170. Medline

Liberman MC (1980) Morphological differences among radial afferent fibers in the cat cochlea: an electron-microscopic study of serial sections. Hear Res 3:45–63. CrossRef Medline

Mainen ZF, Sejnowski TJ (1996) Influence of dendritic structure on firing pattern in model neocortical neurons. Nature 382:363–366. CrossRef Medline

Makara JK, Losonczy A, Wen Q, Magee JC (2009) Experience-dependent compartmentalized dendritic plasticity in rat hippocampal CA1 pyramidal neurons. Nat Neurosci 12:1485–1487. CrossRef Medline

McLean WJ, Smith KA, Glowatzki E, Pyott SJ (2009) Distribution of the Na, K-ATPase alpha subunit in the rat spiral ganglion and organ of corti. J Assoc Res Otolaryngol 10:37–49. CrossRef Medline

Nayagam BA, Muniak MA, Ryugo DK (2011) The spiral ganglion: connecting the peripheral and central auditory systems. Hear Res 278:2–20. CrossRef Medline

Nouvian R, Beutner D, Parsons TD, Moser T (2006) Structure and function of the hair cell ribbon synapse. J Membr Biol 209:153–165. CrossRef Medline

Pan E, Colbert CM (2001) Subthreshold inactivation of Na+ and K+ channels supports activity-dependent enhancement of back-propagating action potentials in hippocampal CA1. J Neurophysiol 85:1013–1016. Medline

Perkins RE, Morest DK (1975) A study of cochlear innervation patterns in cats and rats with the Golgi method and Nomarkski optics. J Comp Neurol 163:129–158. CrossRef Medline

Pongracz F, Firestein S, Shepherd GM (1991) Electrotonic structure of olfactory sensory neurons analyzed by intracellular and whole cell patch techniques. J Neurophysiol 65:747–758. Medline

Rapp M, Yarom Y, Segev I (1996) Modeling back propagating action potential in weakly excitable dendrites of neocortical pyramidal cells. Proc Natl Acad Sci U S A 93:11985–11990. CrossRef Medline

Robertson D (1976) Possible relation between structure and spike shapes of neurones in guinea pig cochlear ganglion. Brain Res 109:487–496. CrossRef Medline

Robertson D (1984) Horseradish peroxidase injection of physiologically characterized afferent and efferent neurones in the guinea pig spiral ganglion. Hear Res 15:113–121. CrossRef Medline

Robertson D, Sellick PM, Patuzzi R (1999) The continuing search for outer hair cell afferents in the guinea pig spiral ganglion. Hear Res 136:151–158. CrossRef Medline

Romand MR, Romand R (1987) The ultrastructure of spiral ganglion cells in the mouse. Acta Otolaryngol 104:29–39. CrossRef Medline

Romand R, Romand MR (1984) The ontogenesis of pseudomonopolar cells in spiral ganglion of cat and rat. Acta Otolaryngol 97:239–249. CrossRef Medline

Rutherford MA, Chapochnikov NM, Moser T (2012) Spike encoding of neurotransmitter release timing by spiral ganglion neurons of the cochlea. J Neurosci 32:4773–4789. CrossRef Medline

Simmons DD, Liberman MC (1988) Afferent innervation of outer hair cells in adult cats: I. Light microscopic analysis of fibers labeled with horseradish peroxidase. J Comp Neurol 270:132–144. CrossRef Medline

Slugg RM, Meyer RA, Campbell JN (2000) Response of cutaneous A- and C-fiber nociceptors in the monkey to controlled-force stimuli. J Neurophysiol 83:2179–2191. Medline

Spoendlin H (1967) The innervation of the organ of Corti. J Laryngol Otol 81:717–738. CrossRef Medline

Spoendlin H (1969) Innervation patterns in the organ of Corti of the cat. Acta Otolaryngol 67:239–254. CrossRef Medline

Spoendlin H (1971) Degeneration behaviour of the cochlear nerve. Arch Klin Exp Ohren Nasen Kehlkopfheilkd 200:275–291. CrossRef Medline

Spoendlin H (1972) Innervation densities of the cochlea. Acta Otolaryngol 73:235–248. CrossRef Medline

Spruston N, Schiller Y, Stuart G, Sakmann B (1995) Activity-dependent action potential invasion and calcium influx into hippocampal CA1 dendrites. Science 268:297–300. CrossRef Medline

Stuart GJ, Sakmann B (1994) Active propagation of somatic action potentials into neocortical pyramidal cell dendrites. Nature 367:69–72. CrossRef Medline

Stuart G, Spruston N, Sakmann B, Häusser M (1997) Action potential initiation and backpropagation in neurons of the mammalian CNS. Trends Neurosci 20:125–131. CrossRef Medline

Van Hees J, Gybels JM (1972) Pain related to single afferent C fibers from human skin. Brain Res 48:397–400. CrossRef Medline

Weisz C, Glowatzki E, Fuchs P (2009) The postsynaptic function of type II cochlear afferents. Nature 461:1126–1129. CrossRef Medline

Weisz CJ, Lehar M, Hiel H, Glowatzki E, Fuchs PA (2012) Synaptic transfer from outer hair cells to type II afferent fibers in the rat cochlea. J Neurosci 32:9528–9536. CrossRef Medline

Yi E, Roux I, Glowatzki E (2010) Dendritic HCN channels shape excitatory postsynaptic potentials at the inner hair cell afferent synapse in the mammalian cochlea. J Neurophysiol 103:2532–2543. CrossRef Medline

Yoshimura M, Jessell TM (1989) Primary afferent-evoked synaptic responses and slow potential generation in rat substantia gelatinosa neurons *in vitro*. J Neurophysiol 62:96–108. Medline

Young ED (2010) Level and spectrum. In: Oxford handbook of auditory science, vol. 2: the auditory brain, Section 2: Information coding in the auditory brain: sound identification (Palmer A, Rees A, eds.), pp 93–124. London: Oxford UP.